JCEC
THE JOURNAL OF ENGINEERING AND EXACT SCIENCES

OPEN ACCESS

The Journal of Engineering and Exact Sciences – jCEC, Vol. 08 N. 06 (2022)
journal homepage: https://periodicos.ufv.br/jcec
eISSN: 2527-1075
ISSN: 2446-9416

Numerical simulation of forced convective fish drying performance of different cabinet geometry

Article Info:
Article history: Received 2022-06-16 / Accepted 2022-09-01 / Available online 2022-09-12
doi:

Joshua Kolawole Gbegudu
ORCID: https://orcid.org/0000-0003-2417-2520
University of Lagos, Nigeria
E-mail: jk.gbegudu@gmail.com
Ibrahim Ademola Fetuga
ORCID: https://orcid.org/0000-0002-1943-4234
University of Lagos, Nigeria
E-mail: fetugaebraheem@gmail.com
Olabode Thomas Olakoyejo
ORCID: https://orcid.org/0000-0001-9942-1339
University of Lagos, Nigeria
E-mail: oolakoyejo@unilag.edu.ng
Manasseh Babale Shitta
ORCID: https://orcid.org/0000-0001-6070-5748
University of Lagos, Nigeria
E-mail: shitta@nceec.gov.ng
Antônio Marcos de Oliveira Siqueira
ORCID: https://orcid.org/0000-0002-7088-3211
Federal University of Viçosa, Brazil
E-mail: antonio.siqueira@ufv.br
Emmanuel Obiani Akari
ORCID: https://orcid.org/0000-0001-5910-4144
University of Lagos, Nigeria
E-mail: akariobiani42@gmail.com
Kolade Sodeeq Aderemi
ORCID: https://orcid.org/0000-0003-2073-1145
University of Lagos, Nigeria
E-mail: sodeeqkolade@yahoo.com

Abstract
Two forced convective fish rotary dryers of different geometries (cube and cylindrical) with modelled fish were simulated using ANSYS commercial software to determine the geometry that gives an optimal inlet temperature distribution profile, which ultimately leads to faster drying of fish. The geometries were constructed using CATIA V5 modelling software such that they both have the same volume, so they can be compared appropriately. The simulation was carried out for different inlet temperatures and at different time intervals. From the simulations carried out, it was discovered that the cylindrical rotary dryer possesses the maximum mean dryer temperatures in most of the time intervals considered. The temperature distribution obtained thus reveals that the cylindrical d duration of thermal action on the products. Therefore, the cylindrical rotary dryer gives an increased drying rate and an improved quality of product.
Keywords: Computational fluid dynamics. Shape optimization. Cube shape dryer. Cylindrical rotary dryer.

1. Introduction

Drying is a very important process in the food industry for the preservation of food over a very long period. Fish drying is used to preserve fish so as to have a storage life of several years without losing taste and quality. It involves moving the moisture content to the surface of the product and subsequently evaporating it by thermal heating (Hedayati et al., 2020; Van Rooyen et al., 2022). There are different ways in which fish can be dried, which include open sun drying, fuel dependent drying, electrical drying, solar drying and much more, but we know the most common drying of fish in Nigeria is open air drying and fuel dependent drying, which comes with a lot of disadvantages like: requiring a large open surface area exposed to direct sunlight and consequent contamination of the fish product. Fuel dependent drying using firewood and charcoal can be very carcinogenic as the smoke from the wood and charcoal comes into direct contact with the product. These methods can lead to uneven drying of the product, which can lead to the growth of microorganisms, and subsequently to food poisoning, which is very dangerous for human health. Contamination of the food product through contact with dust, rodents, insects and birds can also cause the product to decompose, be of lower quality and be very unhealthy for consumption (Ezzatpanah et al., 2022; Vijayan, Arjunan, and Kumar, 2016).

Aside from the conventional method used for drying and preserving fish, forced convection cabinet drying is one of the effective preservation techniques for fish, since proper preservation methods are important for maintaining a constant food supply to the population while also maintaining and retaining its taste and quality. Forced convective cabinet drying has a lot of advantages over the other types of drying, which include: simplicity in terms of construction, uniform drying capabilities, and it dries from the inside out, more effective and shorter time required for drying, protection from contamination, availability throughout the year in all weather conditions, and improved product quality (Ahmadi et al., 2021; Getahun et al., 2021; Kamarulzaman, Hasanuzzaman, and Rahim, 2021). The limitation of cabinet drying is the non-uniformity of the final moisture content of products. These limitations are minimized with adequate cabinet drying design to improve the airflow velocity distribution and temperature uniformity in the dryer. Good drying can reduce post-harvest losses and increase the production and storage life of the products.

Much research has been done to examine the different methods of drying foods such as fruits, vegetables, and seafood. Researchers like (Paraschiv, Ion, and Paraschiv, 2011) developed and validated a model of the thermodynamic performance of parabolic trough solar collectors (PTLC) employed in a macro-combined cooling, heating, and power (MCCHP) system. (Tunde-Akintunde and Afon, 2010) investigated with Fick's diffusion model the effects of pre-treatment on cassava chips dried in a hot–air dryer at a temperature of 60^{o}C and constant air velocity of 1.5m/s. (Kaya, Aydin, and Dincer, 2008)used a finite difference method with convective boundary conditions at the object's surfaces to study mass and heat transfer of an observed object in two dimensions, reporting, among other things, that the corrective coefficients at one side wall of the object were higher than at the other sides due to peculiarities of air upstream. Especially since higher aspect ratios guarantee a longer drying period than smaller aspect ratios. In 2008, (Sreekumar, Manikantan, and Vijayakumar, 2008) discovered that exposing fish products directly to sunlight will decrease the quality of the product via discoloration, undesirable temperature rises at the surface, and inadequate internal drying, i.e., fish does not dry from the inside out. (Margaris and Ghiaus, 2006) numerically studied the processes in the drying chamber and experimentally validated the model with a single tray in the drying chamber and discovered that the standard $k{-}\varepsilon$ model is the most effective turbulent model. (Weiss and Buchinger, 2002) reported that the free convective dryer typically exhibits lower overall drying efficiencies of about 10-15% than the forced convection model by about 20–30%. (Torres-Reyes, Navarrete-Gonzalez, and Ibarra-Salazar, 2002) used semi-empirical models to study the thermal performance analysis of the cabinet type indirect solar dryer for mango slices. From the study, it was discovered that products placed at a higher position had higher humidity as compared to products placed at a lower position, and there was improved drying with an increase in the flow rate of inlet air. (Karathanos and Belessiotis, 1997) developed a solar

dryer on a large scale with a propane gas burner for an artificial drying system, which showed a significant reduction in drying time than that for solar radiation (Doe and Heruwati, 1988) devised a computer model application for both traditional and mechanical drying of fish. The model could predict the effects of change with a certain level of confidence over a range of climatic conditions. (Akari et al., 2022) adopted a numerical approach to determine the best inlet air temperature for forced convective fish cabinet rotary dryer. They considered the air inlet temperature of 35^{o}C to 55^{o}C and time of 0min to 120min. It was found from the results that the optimum conditions to achieve an effective fish drying process take place at the air inlet temperature of 55^{o}C and time of 70 min.

Although there are number of research work on drying, however few reported on the use of ANSYS for reporting the performance of the drying process based on different geometry. Hence, the need to work on a dryer that has a geometry that can increase our drying rates without reducing the quality of the product in terms of taste, appearance, and color than may be obtainable in other methods of drying. This study is focusing on comparing various dryer geometries through numerical simulations using ANSYS CFX to effectively predict the dryer geometry that will give us an optimal result.

2. Methodology

Computational fluid dynamics (CFD) was applied in the analysis of the effect of fish dryer geometry on the drying of fish. This required the creation of all the geometries that contain the control volumes of the entire dryer assembly. Both dryer geometries were modelled using CATIA V5 3D modelling software and the individual parts were exported in the initial graphic specification (IGS) format for further processing in ANSYS Workbench. The computational grid elements (mesh) of all domains are created using the ANSYS ICEM CFD Mesher with the application of the relevant mesh settings that enable the suitability of the mesh to the domain physics. The individual meshes are now exported and saved for further processing in ANSYS CFX. The boundary conditions, domains, domain interfaces, solver settings, and material properties of the fish and the air for both dryer geometries are setup in ANSYS CFX. Prior to the commencement of the transient simulation, a steady-state simulation is performed. This procedure is necessary for the derivation of the initial boundary values for all domains and flow quantities (temperature, pressure, velocity). The transient simulation was actualized by varying the time in increments of 10 minutes. The first simulation was carried out at 10 mins and then increased gradually till it got to 120 mins for different inlet drying temperatures, which varied from 35 degrees Celsius to 55 degrees Celsius for both dryer cases.

2.1 Geometry Description

Two rotary dryer geometries with uniform volumetric capacity are considered in this CFD analysis. The first dryer geometry, as shown in Figure 1, is a cube-shaped rotary dryer, while the second dryer geometry, as shown in Figure 2, is a cylindrical-shaped rotary dryer. Both dryers are fed with hot air through their circular inlets with the aid of a heat pump at a specific air speed. The hot air is further distributed around the fish by means of the rotating table, which helps to carry the fish during the drying process. Table 1. summarizes the details of the dimensions for both the cube-shape and the cylindrical dryer.

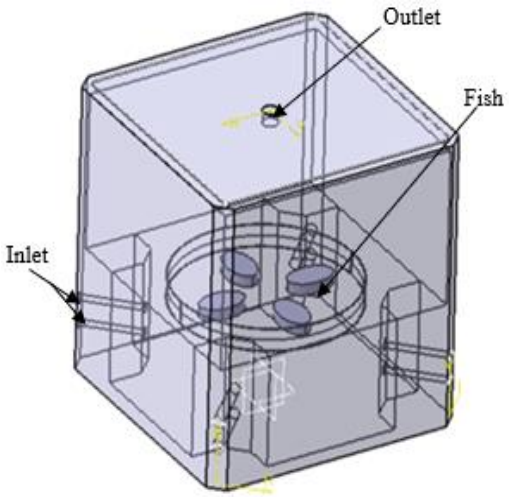

Figure 1- Cube shape rotary dryer

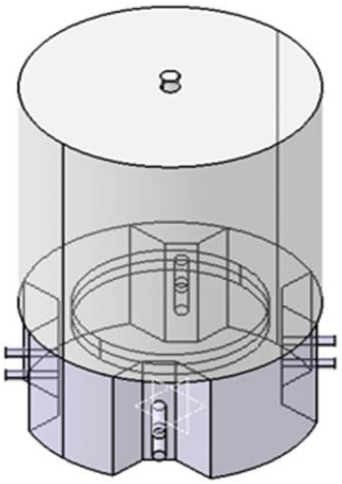

Figure 2- 3D view of Computational domain

Table 1- Dimensions of the dryers used for the computational fluid dynamics study

Parameters	Cube Shape Rotary Dryer	Cylindrical Rotary Dryer
Dimension	1m length x 1m width x 1m height	1m diameter x 1.338m height
Gross rotary dryer volume	$1m^3$	$1m^3$
Net Volume of rotary dryer (Volume of internal fluid region)	0.76 m^3	0.76 m^3
Number of inlets	8	8
Diameter of each inlet	0.04m	0.04m
Number of outlets	1	1
Internal fluid in dryer before drying process	Air at 25C	Air at 25C

2.2 Mesh Generation

As shown in Figure 3(a) through 3(c), the computational grid or mesh for both dryer geometries were created using the ANSYS ICEM CFX Mesher. The meshing was carried out on all computational domains and saved individually for later processing. The flow physics in some distinct geometries, such as edges, concentric faces, and smaller openings, was captured using the Automatic Inflation feature settings. The mesh elements generated include tetrahedral, pyramids, wedges, and hexahedral element types. The overall mesh quality of all the dryer domains was high, and this was ensured to obtain a good prediction of the flow.

Figure 3(a)- Grid of the cube shape dryer (fluid domain) 3(b) Grid of the fish (solid domain) 3(c) Grid of the cylindrical dryer (fluid domain) 3(d) Grid of the fish boundary (fluid domain)

2.3 Problem Formulation

The governing equations, boundary conditions, and assumptions employed are discussed in this section. The unsteady Navier-Stokes equations in their conservation form are the set of equations solved by ANSYS CFX. The assumptions considered in the simulation of the drying process are as follows:

1. The flow of hot air into the chamber is considered to be a turbulent flow, transient, and 3-dimensional flow.
2. The initial temperature inside the dryer is assumed to be ambient prior to the commencement of the drying process.
3. Both dryer geometry configurations are assumed to be of equal volumetric capacities.
4. The drying air is incompressible and of low Mach number.
5. The effect of radiation is negligible.
6. The shape of the product is unaltered during the drying process.
7. The rotary table is assumed to be fully porous for maximum flow of hot air to the fish.
8. No-slip velocity boundary condition at the wall of the air within the chamber.

We can obtain the continuity equation, momentum equation, and energy equation as expressed below using the mass, momentum, and energy conservation principles.

Continuity equation

$$\frac{D\rho}{Dt} + \rho \frac{\partial U_i}{\partial x_i} = 0 \tag{1}$$

Momentum equation

$$\rho \frac{\partial U_j}{\partial t} + \rho U_i \frac{\partial U_j}{\partial x_i} = -\frac{\partial P}{\partial x_j} - \frac{\partial \tau_{ij}}{\partial x_i} + \rho g_j \tag{2}$$

where $\tau_{ij} = -\mu\left(\frac{\partial U_j}{\partial x_i} + \frac{\partial U_i}{\partial x_j}\right) + \frac{2}{3}\delta_{ij}\mu \frac{\partial U_k}{\partial x_k}$ (3)

Energy equation

$$\rho c_\mu \frac{\partial T}{\partial t} + \rho c_\mu U_i \frac{\partial T}{\partial x_i} = -P \frac{\partial U_i}{\partial x_i} + \lambda \frac{\partial^2 T}{\partial x_i^2} - \tau_{ij} \frac{\partial U_j}{\partial x_i} \tag{4}$$

Turbulence equation
k-epsilon turbulence model
In the $k - \varepsilon$ model, two new variables are included into the system of equations. The turbulence kinetic energy is denoted by k, and the rate at which velocity fluctuations dissipate is denoted by ε. The continuity equation is further written as follows:

$$\frac{\partial \rho}{\partial t} + \frac{\partial}{\partial x_j}\left(\rho U_j\right) = 0 \tag{5}$$

and the momentum equation is then:

$$\frac{\partial p U_i}{\partial t} + \frac{\partial}{\partial x_j}\left(\rho U_i U_j\right) = -\frac{\partial P'}{\partial x_i} + \frac{\partial}{\partial x_j}\left[\mu_{eff}\left(\frac{\partial U_i}{\partial x_j} + \frac{\partial U_j}{\partial x_i}\right)\right] + S_M \tag{6}$$

Where the sum of body forces is represented by S_M, effective viscosity accounting for turbulence is denoted by μ_{eff} and the modified pressure is denoted by P'. Thus, $\mu_{eff} = \mu + \mu_t$
where turbulence viscosity is represented by μ_t. The $k - \varepsilon$ model implies that turbulence viscosity is proportional to turbulence kinetic energy and dissipation, as follows:

$$\mu_t = C_\mu \rho \frac{k^2}{\varepsilon} \tag{7}$$

Thus,

$$\frac{\partial(\rho k)}{\partial t} + \frac{\partial}{\partial x_j}\left(\rho U_j k\right) = \frac{\partial}{\partial x_j}\left[\left(\mu + \frac{\mu_t}{\sigma_k}\right)\frac{\partial k}{\partial x_j}\right] + P_k - \rho\varepsilon + P_{kb} \tag{8}$$

$$\frac{\partial(\rho \varepsilon)}{\partial t} + \frac{\partial}{\partial x_j}\left(\rho U_j \varepsilon\right) = \frac{\partial}{\partial x_j}\left[\left(\mu + \frac{\mu_t}{\sigma_\varepsilon}\right)\frac{\partial \varepsilon}{\partial x_j}\right] + \frac{\varepsilon}{k}(C_{\varepsilon 1} P_k - C_{\varepsilon 2}\rho\varepsilon + C_{\varepsilon 1} P_{\varepsilon b}) \tag{9}$$

where $C_{\varepsilon 1}$, $C_{\varepsilon 2}$, σ_k and σ_ε are constants.

The influence of the buoyancy forces, which are expressed below, is represented by P_{kb} and $P_{\varepsilon b}$. P_k is the turbulence produced by viscous forces, which is expressed as follows;

$$P_k = \mu_t \left(\frac{\partial U_i}{\partial x_j} + \frac{\partial U_j}{\partial x_i}\right)\frac{\partial U_i}{\partial x_j} - \frac{2}{3}\frac{\partial U_k}{\partial x_k}\left(3\mu_t \frac{\partial U_k}{\partial x_k} + \rho k\right) \quad (10)$$

Table 2- Material properties for the air, fish, and dryer body

Material Name	(Air at 25°C) Ambient Air	Fish	Dryer body
Material Description	Air at 25°C and 1 atm (dry)	Tropical Fish	Steel
Thermodynamic state	Gas	Solid	Solid
Molar Mass (kg/kmol)	28.96	178.976	55.85
Density (kg/m^3)	1.185	1055	7854
Specific Heat Capacity (Jkg^{-1}K^{-1})	1004.4	3540	4340
Dynamic viscosity (kgm^{-1}s^{-1})	1.832×10^{-5}	-	-
Thermal conductivity (Wm^{-1}K^{-1})	2.61×10^{-5}	0.282744	60.5
Buoyancy properties (K^{-1})	0.003356	-	-

Boundary Conditions

Domains

The domains setup for both rotary dryer configurations was done for each fluid /solid zones as described below.

Internal Air Volume (Fluid Domain)

The descriptions of the domain settings for the inner air fluid domain, fish solid domain, fish boundary fluid domain and domain interface as inputted in CFX-Pre are listed in the Table 3 and Table 4 below:

Table 3- Domain settings and Boundary conditions for the internal air volume, fish boundary and fish domain

	Internal Air Volume	**Fish Boundary Fluid Domain**	**Fish Solid Domain**
Domain type	Fluid domain	Fluid domain	Solid domain
Material	Air at 25ºC	Air at 25ºC	Fish
Morphology	Continuous fluid	Continuous fluid	Continuous Solid
Reference pressure	1 atm	1 atm	1 atm
Buoyancy model	Non buoyant	Non buoyant	Non buoyant
Domain motion	Stationary	Rotating ω =5 rev/min at coordinate axis of Global Y	Rotating ω =5 rev/min at coordinate axis of Global Y
Mesh deformation	None	None	None
Heat transfer	Total Energy	Total Energy	Thermal Energy
Turbulence	K-Epsilon	K-Epsilon	-
Wall function	scalable	scalable	-

Domain Interface

The domain interface was created to serve as an interface for the exchange of momentum and energy flow quantities between the inner air fluid domain (stationary domain) and the rotating fluid domain (fish boundary domain). This is to enable the conservation of the thermodynamic flow quantities, viz., momentum, mass, and energy, across the different domain boundaries. The description of the domain interface settings is listed below.

Table 4- Domain settings and Boundary conditions for the inner air fluid- fish boundary interface

Inner Air Fluid Domain – Fish Boundary Domain Interface	
Interface Type	Fluid – Fluid
Interface name	Inner Air region – Fish boundary domain interface
Interface side 1	Inner Air Fluid Domain
Interface side 2	Fish Boundary
Interface models	General connection
Frame Change/Mixing Model	Frozen Rotor
Pitch Change (option)	Specified pitch angles
Pitch angle side 1	360 degrees
Pitch angle side 2	360 degrees
Additional Interface models	Mass and Momentum (Conservative interface flux) Interface model (none)
Mesh Connection	GGI

3. Numerical Procedure

The CFX-Solver settings inputted for the simulation include the advection scheme, transient scheme, turbulence numeric and output transient results settings. The convergence control for both minimum and maximum coefficient loops was given as 1 and 10 respectively, while the timescale control is set as Coefficient Loops. The convergence criteria were set at 10^{-4}. At the commencement of the simulation, an initial values file was imported from a previous steady state simulation after one (1) iteration. This served as a starting point for the solver in predicting the flow field quantities (temperature, velocity, and pressure).

4. Results and Discussions

On completion of the simulation, the temperature distribution of the air (fluid domain) within the drier at different inlet air temperatures and time intervals was obtained. The three different inlet temperatures of 35ºC, 45ºC, and 55ºC were simulated for a time interval of 10 minutes to 120 minutes to ascertain the dryer that would attain the optimum drying temperature range faster. The range of drying temperatures within the two rotary dryers must be suitable enough to dry the fish efficiently without causing damage to the fish. To be analyzed is the optimum geometrical configuration that would provide sufficient heat distribution around the fish.

4.1 Mean Drying Temperature Result Analyses

The mean drying temperatures attained by both dryers for three inlet temperatures and drying times are highlighted as shown in Table 5. The mean drying temperatures are compared. Maximum mean dryer temperatures after 30 min: The cylindrical dryer has the highest mean drying temperatures of all the three inlet air temperatures (35ºC, 45ºC, and 55ºC) after thirty minutes of operation. Maximum mean dryer temperatures after 60 min: The mean drying temperature of the cylindrical dryer is slightly higher than that of the cube shaped dryer for two inlet air temperatures only (45ºC and 55ºC). The cube-shaped dryer temperature was only higher for the 35ºC inlet air. Maximum mean dryer temperatures after 90 min: The cylindrical dryer possesses the highest mean drying temperatures for the two inlet air temperatures of 45ºC and 55ºC while the cube-shaped dryer has the highest mean drying temperatures for 35ºC only. Maximum mean dryer temperatures after 120 min: The mean drying temperature of the cylindrical dryer is slightly higher than that of the cube-shaped dryer for two inlet air temperatures only (45ºC and 55ºC). The cube-shaped dryer temperature was only higher for the 35-degree Celsius inlet air. Figures 4 through 6 show the plot of mean drying temperature versus the drying time at 35ºC, 45ºC, and 55ºC air inlet temperature for cube shape and cylindrical rotary dryer. As for 35ºC air inlet temperature, the mean drying temperature decreases as drying time increases from 0 to 10min and further increases with drying time for both dryers. While for 45ºC, and 55ºC air inlet temperature, the mean drying temperature increases as drying time increases from 0 to 120min.

From the deductions summarized above, it can be understood that the cylindrical rotary dryer possesses the maximum mean dryer temperatures in almost all-time intervals considered. The temperature distribution obtained thus reveals that the cylindrical dryer has better convective air distribution than the cube shaped dryer.

Table 5- Cube shape and Cylindrical rotary results summary

	35ºC (308K) INLET TEMP			45ºC (318K) INLET TEMP			55ºC (328K) INLET TEMP		
	Mean Drying Temperature (K)		Mean Temp difference	Mean Drying Temperature (K)		Mean Temp difference	Mean Drying Temperature (K)		Mean Temp difference
TIME (MINS)	Cube T1	Cylindrical T2	T1-T2	Cube T1	Cylindrical T2	T1-T2	Cube T1	Cylindrical T2	T1-T2
0	298.00	298.00	0	298.00	298.00	0	298.00	298.00	0
10	297.96	297.94	0.02	299.27	300.41	-1.14	301.18	302.83	-1.65
20	299.24	299.68	-0.44	301.56	303.56	-2.00	304.46	307.34	-2.88
30	300.72	300.89	-0.17	304.21	305.59	-1.38	308.27	310.25	-1.98
40	302.00	301.85	0.15	306.46	307.27	-0.81	311.49	312.66	-1.17
50	302.89	302.62	0.27	308.06	308.62	-0.56	313.79	314.60	-0.81
60	303.56	303.23	0.33	309.28	309.71	-0.43	315.54	316.17	-0.63
70	304.07	303.72	0.35	310.19	310.56	-0.37	316.85	317.38	-0.53
80	304.45	304.09	0.36	310.87	311.22	-0.35	318.61	318.32	0.29
90	304.73	304.38	0.35	311.38	311.78	-0.4	318.67	319.05	-0.38
100	304.93	304.61	0.32	311.77	312.13	-0.36	319.11	319.62	-0.51
110	305.09	304.79	0.30	312.07	312.44	-0.37	319.54	320.07	-0.53
120	305.21	304.93	0.28	312.29	312.68	-0.39	319.86	320.42	-0.56

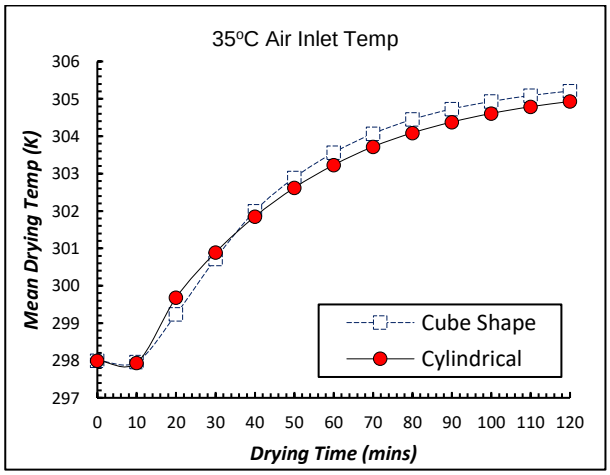

Figure 4- Mean drying temperature against drying time for Cube shape and cylindrical rotary dryer at 35ºC air inlet temp.

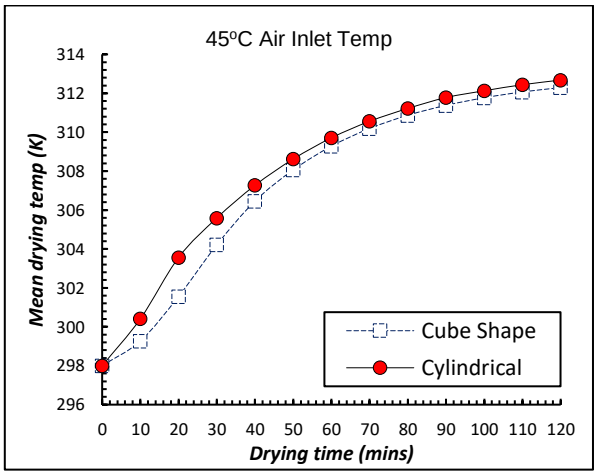

Figure 5- Mean drying temperature against drying time for Cube shape and cylindrical rotary dryer at 45ºC air inlet temp.

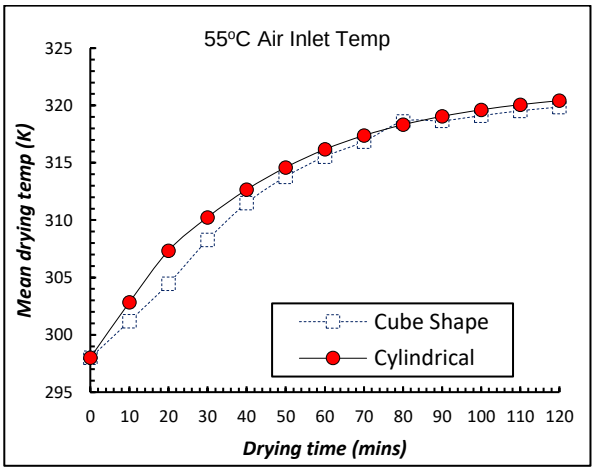

Figure 6- Mean drying temperature against drying time for Cube shape and cylindrical rotary dryer at 55ºC air inlet temp.

4.2 Scatter plot analyses

The scatter plots shown in Figure 7 through 9 show the difference in mean drying temperatures between both rotary dryer configurations at different inlet air temperatures. Plot deflecting towards the left of the axis (negative values) indicates the cylindrical dryer has the highest mean dryer temperatures, while plot deflecting to the right of the axis (positive values) indicates the cube shaped dryer has the highest mean dryer temperatures. According to Figure 7, the cube shape rotary dryer has the highest number of mean drying temperatures (ten plot points) while plot points towards the left of the axis shows the cylindrical rotary dryer has the lowest number of mean drying temperatures (two plot points).

As shown in Figure 8, the cylindrical rotary dryer has the overall highest number of mean drying temperatures (all twelve plot points) while the cube shape rotary dryer has the none. The cylindrical rotary dryer has the highest mean drying temperatures (eleven plot points), while the cube-shaped rotary dryer has the fewest (one plot point), according to Figure 9. The scatter plot comparison between the cube-shaped rotary dryer and the cylindrical dryer further reveals that the cylindrical dryer has better heat distribution within the dryer as compared with the latter. The geometrical configuration of both rotary dryers plays a good role in the efficient distribution of heat within the dryer. A faster drying rate requires efficient heat circulation within the dryer. The cylindrical rotary dryer has been considered the ideal dryer of the two rotary dryer configurations due to its high mean drying temperatures at various time intervals. The presence of the rotary table is also of notable interest since it enables the effective circulation of hot air within the dryers, thus improving overall convective heat transfer.

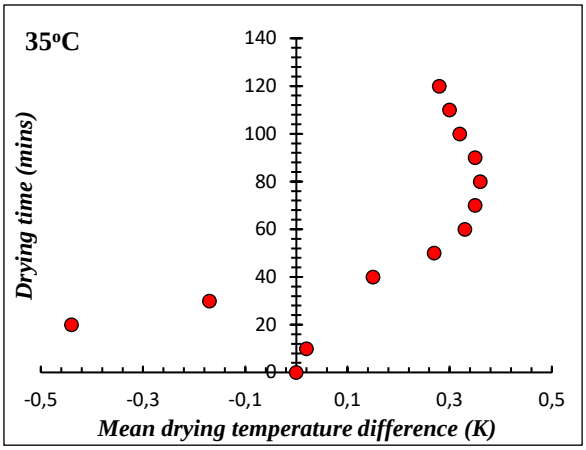

Figure 7- Mean drying temperature difference against drying time at 35ºC air inlet temperature

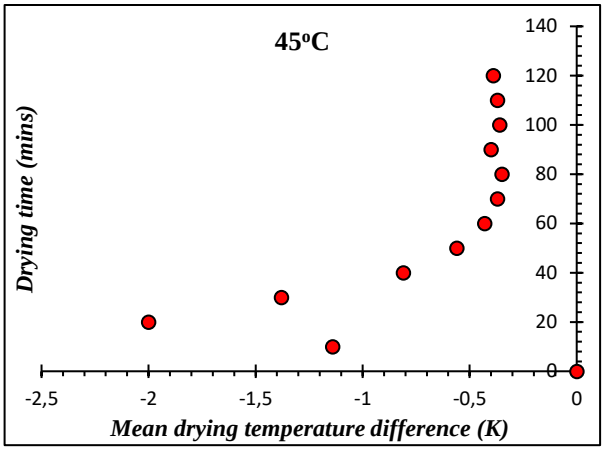

Figure 8- Mean drying temperature difference against drying time at 45ºC air inlet temperature

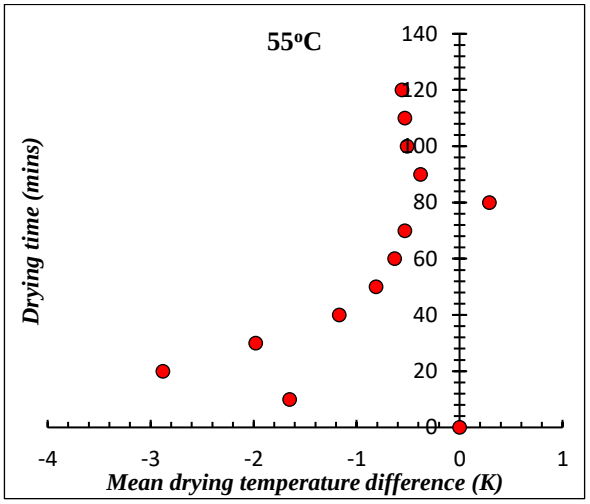

Figure 9- Mean drying temperature difference against drying time at 55ºC air inlet temperature

4.3 Temperature contours

As shown in Figures 10 through 14, The temperature distribution contour plots obtained for the various inlet air temperatures along the center of the dryer (YZ plane, X=0m) for both the cube shape rotary dryer and the cylindrical rotary dryer are shown below;

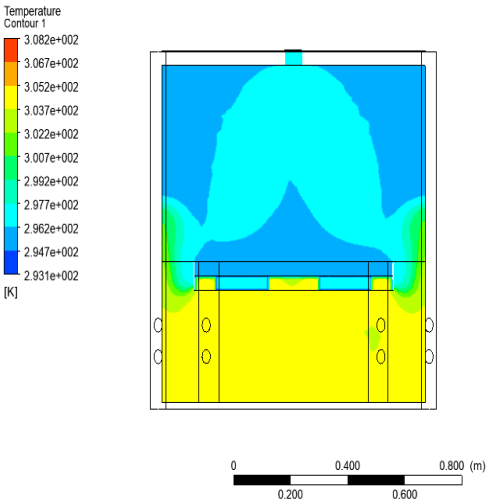

Figure 10: Cube dryer for 35°C, T=20mins, X=0m

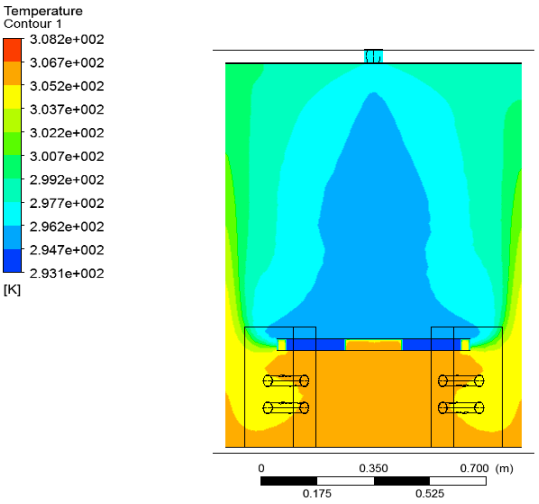

Figure 11: Cylindrical dryer for 35°C, T=20mins, X=0m

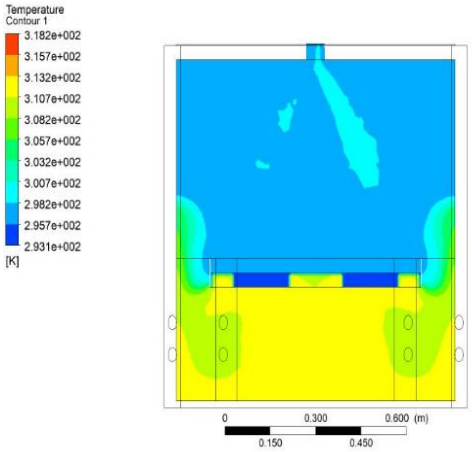

Figure 12: Cube Shape dryer for 45°C, T=20mins, X=0m

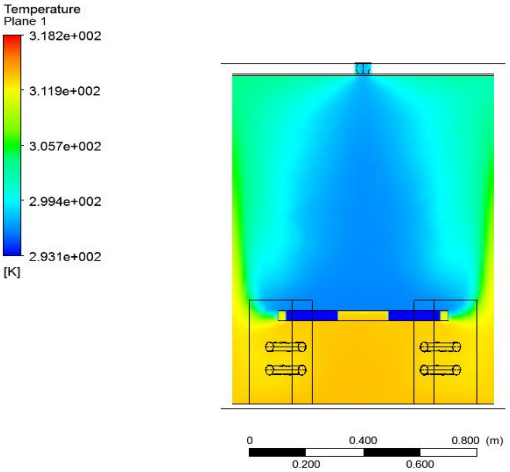

Figure 13: Cylindrical dryer for 45°C, T=20mins, X=0m

5. Conclusion

The relevance of shape and design optimization in the construction of drying plants for fish is of great importance. Sufficient time and effort must be expended to ensure that the optimal geometric configuration of the fish drying equipment is realized. The cylindrical and cube-shaped rotary dryers are typical mechanical dryers that employ the principle of convective heat transfer in carrying out fish drying. Both utilize the use of the inlet hot air pump and rotating table. Therefore, it is of great interest to ascertain which dryer would achieve a faster drying time and thus conserve time and energy. The use of computational fluid dynamics as a research tool in carrying out such an analysis has enabled a lot of design variations to be made in novel rotary dryer designs. Cylindrical rotary dryers are not common as compared to cube-shaped dryers, which have the typical cabinet design. Hence, further analytical research using computational fluid dynamics (CFD) tools in the optimization of the cylindrical rotary dryer geometry would provide more improvement in the technology of artificial fish drying.

References

Ahmadi, A., Das, B., Ehyaei, M. A., Esmaeilion, F., El Haj Assad, M., Jamali, D. H., … Safari, S. (2021). Energy, exergy, and techno-economic performance analyses of solar dryers for agro products: A comprehensive review. *Solar Energy*, *228*, 349–373. https://doi.org/10.1016/J.SOLENER.2021.09.060

Akari, E. O., Fetuga, I. A., Olakoyejo, O. T., Shitta, M. B., Oluwatusin, O., Gbegudu, J. K., and Siqueira, A. M. de O. (2022). Numerical simulation of optimal inlet air temperature of a forced convective fish cabinet rotary dryer. *The Journal of Engineering and Exact Sciences*, *8*(4), 14157-01e. https://doi.org/10.18540/jcecvl8iss4pp14157-01e

Doe, P., and Heruwati, E. (1988). *Drying and storage of tropical fish: a model for the prediction of microbial spoilage*.

Ezzatpanah, H., Gómez-López, V. M., Koutchma, T., Lavafpour, F., Moerman, F., Mohammadi, M., and Raheem, D. (2022). Risks and new challenges in the food chain: Viral contamination and decontamination from a global perspective, guidelines, and cleaning. *Comprehensive Reviews in Food Science and Food Safety*, *21*(2), 868–903. https://doi.org/10.1111/1541-4337.12899

Getahun, E., Delele, M. A., Gabbiye, N., Fanta, S. W., Demissie, P., and Vanierschot, M. (2021). Importance of integrated CFD and product quality modeling of solar dryers for fruits and vegetables: A review. *Solar Energy*, *220*, 88–110. https://doi.org/10.1016/J.SOLENER.2021.03.049

Hedayati-Mehdiabadi, E., Sarhaddi, F., and Sobhnamayan, F. (2020). Exergy performance evaluation of a basin-type double-slope solar still equipped with phase-change material and PV/T collector. *Renewable Energy*, *145*, 2409–2425. https://doi.org/10.1016/J.RENENE.2019.07.160

Kamarulzaman, A., Hasanuzzaman, M., and Rahim, N. A. (2021). Global advancement of solar drying technologies and its future prospects: A review. *Solar Energy*, *221*, 559–582. https://doi.org/10.1016/J.SOLENER.2021.04.056

Karathanos, V. T., and Belessiotis, V. G. (1997). Sun and artificial air drying kinetics of some agricultural products. *Journal of Food Engineering*, *31*(1), 35–46. https://doi.org/10.1016/S0260-8774(96)00050-7

Kaya, A., Aydin, O., and Dincer, I. (2008). Experimental and numerical investigation of heat and mass transfer during drying of Hayward kiwi fruits (Actinidia Deliciosa Planch). *Journal of Food Engineering*, *88*(3), 323–330. https://doi.org/10.1016/J.JFOODENG.2008.02.017

Margaris, D. P., and Ghiaus, A. G. (2006). Dried product quality improvement by air flow manipulation in tray dryers. *Journal of Food Engineering*, *75*(4), 542–550. https://doi.org/10.1016/J.JFOODENG.2005.04.037

Paraschiv, S., Ion, I., and Paraschiv, L. . (2011). Thermodynamic performance for the solar collector of a micro-combined cooling, heating and power system. *Environmental Engineering & Management Journal (EEMJ)*, *10*(9), 1311–1317.

Sreekumar, A., Manikantan, P. E., and Vijayakumar, K. P. (2008). Performance of indirect solar cabinet dryer. *Energy Conversion and Management*, *49*(6), 1388–1395. https://doi.org/10.1016/J.ENCONMAN.2008.01.005

Torres-Reyes, E., Navarrete-Gonzalez, J. J., and Ibarra-Salazar, B. A. (2002). Thermodynamic method for designing dryers operated by flat-plate solar collectors. *Renewable Energy*, *26*(4), 649–660. https://doi.org/10.1016/S0960-1481(01)00147-1

Tunde-Akintunde, T., and Afon, A. . (2010). Modeling of hot-air drying of pretreated cassava chips | Agricultural Engineering International: CIGR Journal. *Agric Eng Int: CIGR Journal*, *12*(2), 34–41.

van Rooyen, J., Simsek, S., Oyeyinka, S. A., and Manley, M. (2022). Holistic View of Starch Chemistry, Structure and Functionality in Dry Heat-Treated Whole Wheat Kernels and Flour. *Foods 2022, Vol. 11, Page 207*, *11*(2), 207. https://doi.org/10.3390/FOODS11020207

Vijayan, S., Arjunan, T. V., and Kumar, A. (2016). Mathematical modeling and performance

analysis of thin layer drying of bitter gourd in sensible storage based indirect solar dryer. *Innovative Food Science and Emerging Technologies*, *36*, 59–67. https://doi.org/10.1016/J.IFSET.2016.05.014

Weiss, W., and Buchinger, J. (2002). Solar drying-Austrian Development Cooperation. *Cite Weiss, W., and J. Buchinger. "Solar Drying–Austrian Development Cooperation." AEE INTEC, Arbeitsgemeinschft ERNEUERBARE ENERGIE-Institute for Sustainable Technologies*, *19*.